PAET Entry Heating and Heat Protection Experiment

NICK S. VOJVODICH*
NASA Ames Research Center, Moffett Field, Calif.

A description is given of the aerothermo environment and associated thermal response of two low-density (270 and 450 kg/cm^3), elastomeric silicone ablators determined during the entry of the NASA Ames Planetary Atmosphere Experiments Test (PAET) vehicle into the Earth's atmosphere. The vehicle configuration, entry parameters, and associated trajectory variables are presented. Measurements of both the surface convective heat-transfer rate and pressure on the beryllium nose cap are shown to be within 5% of theory. The predicted and measured internal temperatures are compared at various depths in the forebody (Martin ESA-3560HF) and afterbody (Martin SLA-220) heat shields. Significant differences observed between experiment and theory for the afterbody thermal response are examined in relation to existing laboratory data.

Nomenclature

A = surface area, m^2
a = acceleration, Earth g
C_d = drag coefficient
f = frequency, GHz
H = total enthalpy, Mjoule/kg
h = altitude, km
h_s = scale height, $\rho/\rho_{sl} = e^{-h/h_s}$, km
K_1 = constant used in Eq. (1), $= \dfrac{82.54 \text{ w cm}^{1/2}}{\text{cm}^2[\text{km/sec}]^{3.15}[\text{kg/m}^3]^{0.5}}$
K_2 = ratio of local to zero-angle-of-attack stagnation point heating rate $= \dot{q}/\dot{q}_{s,\alpha=0}$
K_3 = ratio of local to zero-angle-of-attack stagnation point pressure
K_4 = constant used in Eq. (6), = 9.86 atm/[(kg/m^3)(km/sec)^2]
M = Mach number
m = mass, kg
n = distance normal to surface, cm
p = pressure, atm
Q = total convective heat load, $Q = \int \dot{q} d\tau$, Mjoule/m^2
$\dot{q}$ = convective heat-transfer rate, w/cm^2
Re = Reynolds number based on free stream conditions and body diameter
R_n = nose radius, cm
S = distance along surface, cm
T = temperature, °C
V = velocity, km/sec
α = angle of attack, deg
β = ballistic coefficient, $m/C_d A$, kg/m^2
Δ = change in quantity
θ = flight-path angle, degrees
μ = molecular weight
ρ = density, kg/m^3
τ = time from launch, sec
Φ = angle measured from axis of symmetry

Subscripts

e = entry
s = stagnation point
sl = sea level
w = wall

Introduction

THE NASA Ames Planetary Atmosphere Experiments Test (PAET)[1] was undertaken to demonstrate in an Earth entry flight that measurements made on board an instrumented probe could be used to accurately reconstruct the structure (density, pressure, and temperature vs altitude) and molecular composition of an unknown planetary atmosphere. The successful operation of the instrument complement throughout the entire entry required heat shielding to protect the probe from the convective heating encountered during the high-speed phase of re-entry. Since two of the instruments, a radiometer and a mass spectrometer, required a contamination-free stagnation region, a beryllium heat sink was selected for the spherical nose region to avoid ablation products. The remainder of the vehicle was to be protected by efficient low-density ablators. It was recognized in the early planning stages of the project that this heat-shield configuration would permit heat-transfer measurements to be made on the beryllium while the external flow property variations were monitored with time. This opportunity would provide an excellent and heretofore unavailable set of conditions for performing a meaningful heat-shield performance experiment. Accordingly, the design and implementation of such an experiment was adopted as an auxiliary PAET objective. This paper is a comprehensive review of the various heat-shield experimental elements including 1) a description of the probe and its entry trajectory; 2) details of the heat sink and heat-shield instrumentation; 3) measurements and predictions of the surface pressure, convective heating rate, and related thermal response of both the forebody and afterbody heat shields; and 4) results from two special tests undertaken to qualify forebody heat-shield penetration and afterbody heat-shield radio-frequency (RF) transparency.

Description of Entry Vehicle and Trajectory

We will begin by briefly discussing those elements of the experiment which directly influenced the aerodynamic heating environment, namely the entry vehicle configuration and trajectory definition measurements.

The blunted, aerodynamically stable, external configuration chosen for the PAET entry vehicle (Fig. 1) was comprised of a forebody and an afterbody. The forebody consisted of a spherical beryllium nose ($R_n = D/2$) with half-angle (Φ) of 35° and a conical frustum of 110°, both attached to an aluminium structural member. The spherical afterbody had a base diameter of

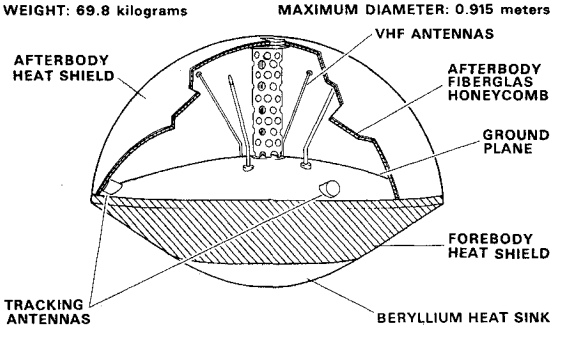

Fig. 1 PAET entry vehicle configuration.

Presented as Paper 72-326 at the AIAA/ASME/SAE 13th Structures, Structural Dynamics, and Materials Conference, San Antonio, Texas, April 10–12, 1972; submitted May 22, 1972; revision received October 16, 1972.

Index categories: Re-Entry Vehicle Testing; Boundary Layers and Convective Heat Transfer—Laminar; Material Ablation.

* Research Scientist.

0.915 m, and its radius center was coincident with the vehicle center of mass to eliminate any destabilizing moments arising from aerodynamic forces acting on its surface. The afterbody ablator was attached to a lightweight fiber-glass honeycomb structure.

Characteristics of the heat shields for the nose, frustum, and afterbody are given in Table 1. As described previously, an aerodynamic consideration dictated the selection of an afterbody that had an extremely large surface area and a corresponding heat shielding weight penalty. Furthermore, the weights of all the components were extremely conservative. No attempt was made to design a minimum-weight heat shield since that heat-shield experiment was considered secondary to the primary mission objectives, and there was boost capability well in excess of the weight associated with the payload alone. The forebody and afterbody heat shields were designed and formulated by the Martin Marietta Corporation,[2] and were bonded to structures fabricated and provided by NASA Ames Research Center. Atmospheric structure instruments were attached to the beryllium and aluminium structure of the forebody; these instruments included on-axis accelerometers, ambient pressure and temperature sensors, a quadrupole mass spectrometer, and an eight-channel radiometer.[3] The VHF antennas for data transmission, the tracking transponders, and the ground plane were located in the afterbody. The afterbody ablator thus had to be capable of transmitting RF signals from the instruments to the ground tracking stations before, during, and after encountering the entry heating pulse.

The PAET spacecraft was launched from NASA, Wallops Island, Va., on June 20, 1971, with a four-stage Scout (S-144 CR) which provided the following nominal entry conditions at an altitude of 90 km: velocity—6.56 km/sec, flight-path angle—40.8°, spin rate—23 rpm, initial angle of attack—28°, and ballistic coefficient—69.8 kg/m^2. Preflight measurements of probe aerodynamic coefficients, the appropriate equations of motion, and the barometric and state equations for the gas environment were used with the information obtained during entry from the prime instrumentation in reconstructing the variation of altitude, velocity, and angle of attack with time (Figs. 2, 3, and 4, respectively).

The analysis of the results was carried out in two steps. For the high-speed portion of the trajectory, during which the probe experienced high rates of deceleration (peak $g = 79$), the only measured quantities required were the three orthogonal components of acceleration. For the low-speed, low-altitude portion of the trajectory, however, the acceleration data had to be complemented by simultaneous measurements of ambient pressure and temperature.[4,5] Figures 2 and 3 also include results from the more conventional method of defining the probe trajectory—namely, radar tracking—along with the estimated uncertainties for both types of measurements.

The PAET atmospheric reconstruction technique provides a direct measurement of the ambient density and thus facilitates calculations of the surface pressure and convective heat-transfer rate. That is, one does not have to assume a standard ARDC-type density profile for the atmosphere or rely on high-altitude atmospheric soundings. The variation of atmospheric density with altitude as deduced from the PAET measurements is shown in Fig. 5. It is interesting to note that the largest deviation between the experimental results and the meteorological data (as was shown for velocity in Fig. 3) occurs at an altitude and time in the trajectory when vehicle peak heating occurs.

Table 1 PAET heat shield compositions and weights

Component	Composition		Density, kg/m^3	Thickness, cm	Weight, kg	Percent of vehicle weight
Spherical nose	Beryllium		1858	1.25	5.44	8.8
Conical frustrum	sr[a]	0.63	450	0.76	3.08	5.0
	sm[b]	0.34				
	sf[c]	0.03				
Spherical afterbody	sr	0.30	270	0.64	2.18	3.5
	sm	0.62				
	sf	0.08				
					Total	17.3%

[a] Silicone resin.
[b] Silica microspheres.
[c] Silica fibers.

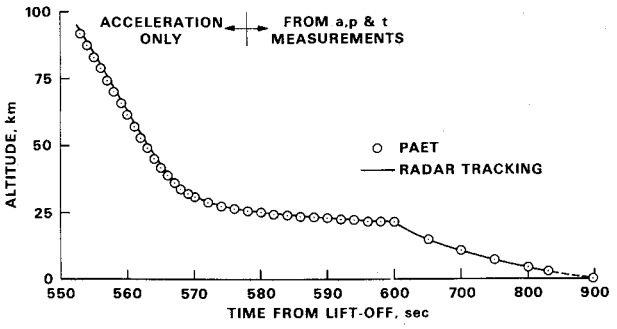

Fig. 2 Variation of deduced altitude with time.

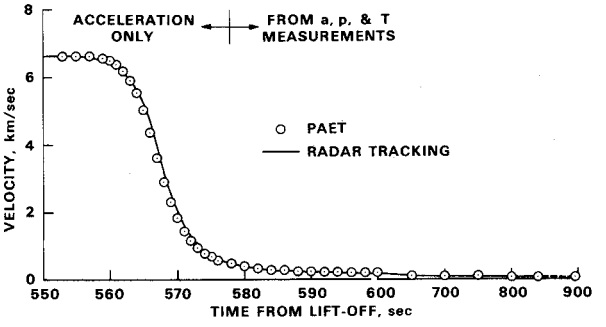

Fig. 3 Variation of deduced velocity with time.

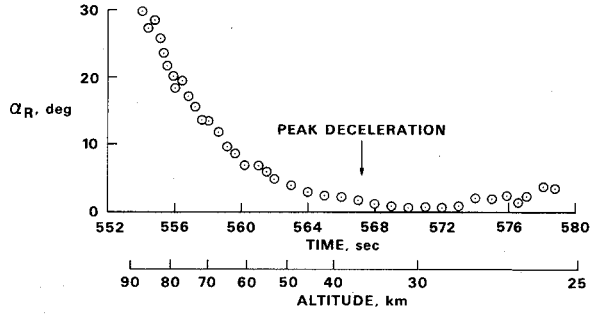

Fig. 4 Variation of vehicle angle of attack with time.

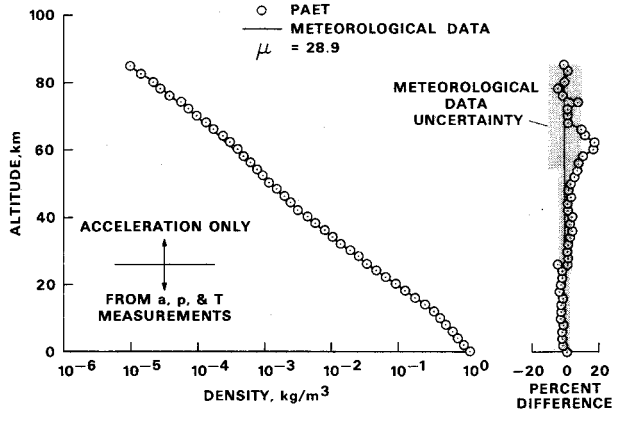

Fig. 5 Variation of deduced density with altitude.

The PAET spacecraft impact occurred 996 sec after launch in the Atlantic Ocean at 33°52′N lat and 64°05′W long, approximately 11 naut miles north of the planned impact point. Recovery of the spacecraft, which was a secondary goal, was not achieved, although aircraft in the recovery zone sighted the vehicle before it sank.

Instrumentation

This section of the paper is concerned with the arrangement of the thermal instrumentation on the vehicle, a description of the data-handling technique used to avoid the blackout problem, and allocation of the respective instrument responses to engineering or storage frame, and it concludes with a description of the construction details of the various thermal sensors.

Instrumentation devoted to the heat-shield experiment comprised six sensors: two beryllium heat-transfer gages, two forebody heat-shield plugs, an afterbody heat-shield thermocouple, and a pressure gage. The arrangement of these sensors on the vehicle is shown in Fig. 6. The heat-transfer gages (A,B) and forebody heat-shield plugs (C,D) were located symmetrically on two rays of the probe to account for the spatial differences induced by vehicle spin and changes in angle of attack. The heat-transfer gages were located as close as possible to the stagnation point ($\Phi = 19°54'$) consistent with the physical dimensions of the radiometer and its quartz window. The forebody heat-shield plugs were situated at the midpoint of the conical section to avoid the analytical complications arising from the presence of the beryllium-ablator interface and the high heating gradients near the shoulder of the vehicle. The afterbody ablator thermocouple was also positioned a sufficient distance downstream of the forebody-afterbody interface. All the instruments were positioned on a common plane, except for the pressure orifice, which was located 16°57′ from the stagnation point on a plane 25° from the other instrumentation. For convenience in discussion, each instrument position has been identified in Fig. 6 by letter.

The communication blackout occurred in the portion of the trajectory of the greatest scientific interest; it is in this high-speed region that the vehicle experiences the highest rates of deceleration and heating. For the PAET entry the blackout lasted from an altitude of 86.2 km–37.7 km with a total elapsed time of 12.2 sec. To overcome the blackout effects, some of the data obtained during the 25.6-sec descent, from 120.7 to 28.9 km, were recorded in a storage frame at a rate of five readings/sec and played back (approximately four times) at the same rate until splashdown. Data from the five thermocouple elements closest to the surface of the forebody and the pressure sensor, which would experience a corresponding rapid response during the blackout, were recorded in the storage frame. The remainder of the thermal data were transmitted from the engineering frame continuously to impact at a rate of one reading per 3.2 sec. The analog outputs of the thermal sensors were converted to a 7-bit digital format by an onboard electronic data signal conditioner and telemetered, by means of the VHF antennas, to receivers at Bermuda, Wallops Island, and the USNS Vanguard. Figure 6 also shows the resolution of each channel of information based on the seven-bit format and maximum range set on the basis of a preflight estimate of the instrument response. The thermocouples, which were chromel alumel, were referenced to a plastic mass deep in the interior of the spacecraft. The temperature of this cold junction was continuously monitored by a thermistor and transmitted as part of the engineering frame data. The initial temperature of this junction was 28.8°C, and at impact it had risen by only 2.4°C.

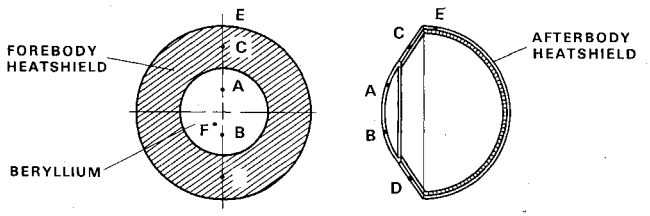

POSITION	COMPONENT	DISTANCE FROM SURFACE n,(cm)	DATA FRAME	RESOLUTION °C	%FS
A	BE	0.025	S	5.1	2.5
B	BE	0.025	S	7.6	2.8
C	F.H.S.	0.330	S,E	9.9	3.3
	F.H.S.	0.635	S	3.2	
	AL	1.02	E	1.9	3.1
D	F.H.S	0.241	S	9.9	1.3
E	A.H.S.	0 .660	E	1.9	2.1
F	BE	0	S,E		

S STORAGE: 1 RDG/0.2 sec
E ENGINEERING: 1 RDG/3.2 sec

Fig. 6 PAET thermal instrumentation; location on vehicle, frame, and sensitivity.

The beryllium heat transfer gages (Fig. 7) were constructed by the High Temperature Instrument Corp., Philadelphia, Pa. (NAS2-5839). The construction technique perfected for the earlier NASA flight heating experiments (Project FIRE[6,7] and Re-entry F[8]) was utilized. To obtain an accurate rapid-response instrument capable of closely following the temperature response of the beryllium heat sink, it was necessary to locate a low-thermal mass thermocouple in immediate contact with the beryllium, as close as possible to the front surface, with a minimum of lead wire conduction loss. This was accomplished by positioning a precooled (−184°C) circular mandrel in a preheated (+255°C) tube; a slot on the periphery of the mandrel contained a slightly oversized thermocouple bead with 0.0025-cm diam leads encased in a twin-bore quartz tube. When the assembly was brought to ambient temperature, a shrink fit occurred between the mating beryllium parts, compressing the thermocouple bead and assuring contact. The top of the mandrel and a portion of the outer cylinder were then machined off, leaving a smooth top surface. The relatively fragile thermocouple wires were connected with larger instrument leads, at a terminal board in the base, and the assembly was potted with a ceramic cement to ensure integrity during launch and entry loadings. The sensor was then X-rayed to accurately define the position of the thermocouple junction relative to the front surface and calibrated prior to installation in the vehicle. In Re-entry F and Project FIRE, the assembled plugs were heat shrunk into the heat sink; for the PAET, however, a shoulder was provided at the bottom of the plug, which mated with a light press fit to a corresponding hole machined in the heat sink. This allowed interchangeability of all plugs, including spares, among the engineering, prototype, and flight vehicles, and reduced the complexity of the assembly. The additional mass contained in this shoulder was accounted for in the analysis. A complete description of the sensor fabrication details is contained in Ref. 8.

The forebody ablation plugs were fabricated, instrumented with thermocouples, and installed in the heat shield by the Martin Marietta Corp., using techniques and methods similar to those previously developed for this class of compliant, elastomeric materials on the Prime Program.[9] A typical plug consisted of

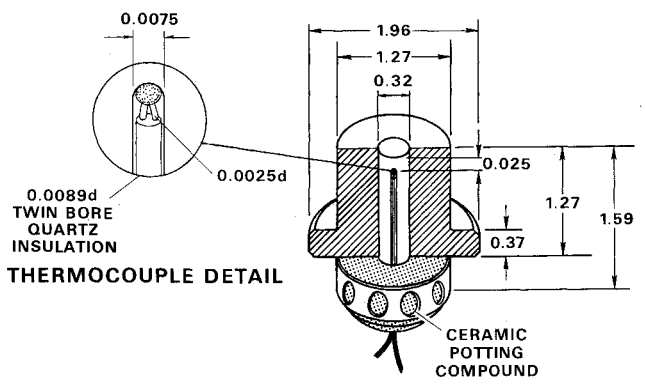

Fig. 7 Beryllium heat-transfer gage.

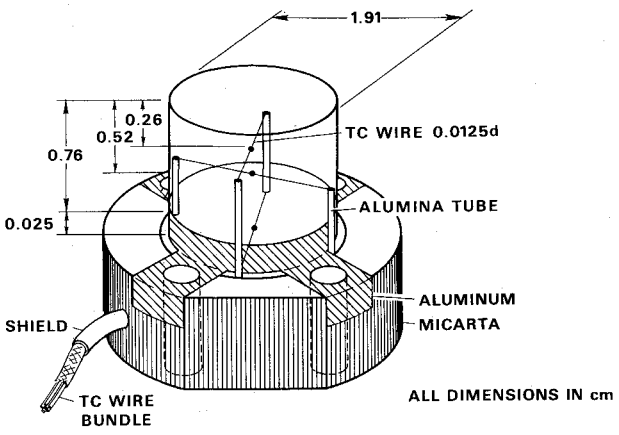

Fig. 8 Forebody heat-shield sensor.

three components (Fig. 8). A cylindrical section of ablator with dimensions matching the thermal capacity of the vehicle structure was bonded to a section of aluminium. At the bottom of the assembly was a tubular micarta base in which the thermocouple lead wires were spliced to the wires leading to the electronic data signal conditioner. The two in-depth thermocouples, located at distances from the surface equivalent to $\frac{1}{3}$ and $\frac{2}{3}$ of the heat-shield thickness, were installed without removing any of the ablator material, as follows: A cylindrical plug of the ablator was installed in a metal die with two opposing holes on an axis parallel to the surface at the two desired depths. One 0.0125-cm-diam thermocouple wire was drawn completely through the die plug, the thermocouple junction was formed outside the die by buttwelding the two dissimilar wires, and the original wire was drawn back into the assembly to a position that located the junction in the vicinity of the cylinder's longitudinal axis. The leads for each thermocouple were brought down the sides of the plug in alumina tubes located in slots on the side of the cylinder (Fig. 8). The third thermocouple was spotwelded to the rear of the aluminium substrate. The micarta base then was filled with a low-conductivity silicone potting compound and tee assembly was X-rayed to accurately define the thermocouple positions. The finished plugs were then attached to the PAET vehicle by means of four screws, and the front surface was sanded to remove any edges and surface discontinuities, and to assure a smooth joint that would not interfere with the quality of the measurement.

To provide for measurement of afterbody temperature, a butt-welded thermocouple was bonded to the outer face sheet of the honeycomb structure with a small patch of fiberglass; the bonding agent and curing process were the same as used in the fabrication of the structure. Therefore, the thermal mass of the system was minimized, and the boundary heating condition did not differ significantly from that of the surrounding structural honeycomb.

The surface pressure on the beryllium heat sink was measured by a vibrating diaphragm transducer[10,11] developed and constructed at NASA Ames Research Center. The sensor determines pressure by monitoring the power required to maintain the resonant vibration of a thin metallic membrane exposed to the test gas. The periodic change in capacitance due to diaphragm motion is measured and converted to an electrostatic force voltage adequate to maintain the desired amplitude. This voltage is related to the gas damping and, hence, pressure. The particularly attractive features of this instrument for flight applications are its absence of zero drift, good dynamic response, and accuracy (2%) over a wide range in pressure (0.001–1 atm).

Aerodynamic Heating Environment

This section deals with two aspects of defining the heating environment of the PAET vehicle during entry: 1) the preflight ground-based tests of scale models to determine the convective heating distribution; and 2) the basic flight data, method of analysis, and comparison of the deduced heating rates and pressure measurements with the theoretical predictions.

Laboratory Results

A one-sixth scale model, of thin-skin construction and instrumented with 17 thermocouples arranged about the periphery, was tested by D. Stewart[12] in two Ames shock tunnel facilities at different angles of attack between 0 and 25°. Reynolds number simulation was not achieved in the tests, but the order-of-magnitude difference in Reynolds number between the two test facilities did not produce a measureable effect in the distribution of heating around the forebody. Figure 9 is a curve fit of the measured ratios of local heating to the heating at the zero-angle-of-attack stagnation point, as a function of normalized distance along the vehicle S/R_n; the data are for the two limiting values of angle of attack, 25° corresponding to the attitude at the beginning of heating and 0° corresponding closely to the attitude (2°) when peak heating was encountered. The position of each thermal sensor is indicated on the abscissa. Early in the entry when the heating rate is low, there is a substantial difference between the levels experienced by the two beryllium heat-transfer gages and the heat shield plugs, with maximum heating occurring near the shoulder. At the peak heating condition the heating rate ratios are 0.88, 0.58, and 0.05 for the heat-transfer gages (A,B), forebody ablation plugs (C,D), and afterbody temperature measurement station (E), respectively. In Ref. 12 the forebody results obtained at zero angle of attack are shown to be in excellent agreement with the theory of Kemp et al.[13] (based on a newtonian pressure distribution) to a point slightly beyond the midpoint of the conical section where the influence of the corner and its subsequent effect on the pressure distribution become important. This observation, with the measurement of shock wave shapes, confirmed that the flow in the region of the spherical nose was governed by the local nose radius and not the cone angle; that is, the effective nose radius for evaluating the heat-transfer rate is equal to the physical nose radius.

Flight Results

The temperature-time history of the two beryllium sensors is shown in Fig. 10; the results are plotted with different origins for purposes of illustration. A careful examination of the results reveals a sinusoidal perturbation on the monotonic instrument response induced by the probe motion as described earlier. Because of the symmetrical sensor deployment on the vehicle, the results are 180° out of phase with the maximum of one measurement corresponding to the minimum of the other.

To obtain the time variation of heating rate to the surface from these in-depth temperature data, the classical inverse boundary value problem for heat conduction was solved using Howard's numerical integration.[14] As a starting point, one first obtains an analytical description of the temperature variation at the measurement station by a smoothing technique. A 21-point walking polynomial of second degree was used with three passes to generate the solid lines shown in Fig. 10. This smoothing

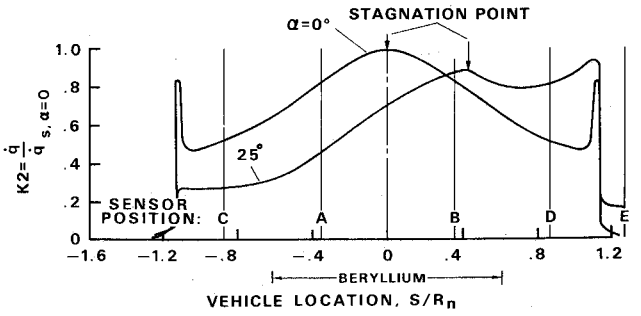

Fig. 9 Sensitivity of PAET convective heating distribution to angle of attack.

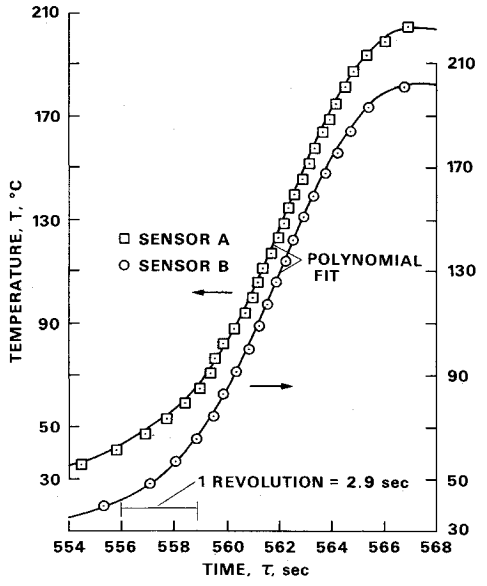

Fig. 10 Measured thermal response of beryllium sensors.

procedure tends to average the sensor response and, accordingly, provides an average heat-transfer rate at each point in time.

The flight heating rates obtained from the analysis described above are shown in Fig. 11 for both sensors along with the theoretical predictions based on the prediction methods of Detra et al.[15] which related the heating rate for a laminar, equilibrium flow boundary layer to the nose radius, and ambient density and vehicle velocity

$$\dot{q} = K_2[K_1\rho^{0.5}V^{3.15}/R_n^{0.5}] \tag{1}$$

The bracketed quantity yields the heat-transfer rate at the stagnation point. The factor K_2, which is the ratio of local to stagnation point for zero angle of attack, is a function of time resulting from the vehicle motion (spin and angle of attack). Two limiting values, corresponding to the most windward and leeward rays, were used to bracket the excursions from the reference value. The level of heating rates obtained with the two sensors under this set of well-defined values of ambient density and vehicle velocity are in good agreement and within 5% of the theory while the heating rate is increasing. The poorer agreement noted later in the trajectory when the heating rate is decreasing is attributable in large measure to the fact that the method of analysis, which is essentially sensitive to the slope of the sensor temperature time history, becomes less accurate as the temperature approaches its peak value.

The heating results are also useful from the atmospheric diagnostic standpoint. By using the simplified trajectory analysis of Allen and Eggers,[16] and with the knowledge of only the entry velocity, initial flight-path angle, ballistic coefficient, and sea level density ρ_{sl}, one can define the velocity and altitude at which peak heating occurs in an atmosphere with a constant scale height, h_s, by means of the following equations:

$$V/V_e = e^{-1/6} = 0.847 \tag{2}$$

$$h = h_s \ln(3h_s\rho_{sl}/\beta \sin\theta_e) \tag{3}$$

The value of velocity at which peak heating occurs [Eq. (2)] is indicated on the abscissa of Fig. 11 and the agreement between experiment and theory is excellent for both sensors. From the times corresponding to this peak for the experiment (563.6 and 563.4 sec) relative to the predicted 563.7[16] and the measured variation of altitude with time, it is possible to evaluate the respective scale heights from Eq. (3). The two values generated by this procedure are within 4.5% of the nominal scale height of 6.7 km for the Earth's atmosphere.

The integrating characteristic of this type of thick-wall beryllium sensor also allows the total heat load

$$Q = \int_0^\tau \dot{q}\, d\tau \tag{4}$$

to be evaluated from the measured final temperature rise and a knowledge of the sensor specific heat variation with temperature and its thermal mass. The value of Q obtained in this manner was 14.98 Mjoule/m^2. The total heat load may also be expressed in terms of the scale height and known entry parameters by using Eq. (4) and a slightly modified form of Eq. (1) in combination with an analytical representation of the density and velocity dependence upon altitude[16]

$$Q = (8.65/10^4)K_1K_2[2h_s\beta/\sin\theta_e]^{1/2}[V_e^2/R_n^{0.5}] \tag{5}$$

Equation (5) yields a value for the total heat load of 15.47 MJ/m^2 which is within 4% of the measurement. This predicted value represents approximately 2% of the entry vehicle's initial kinetic energy, $1/2\, mV_e^2$.

Measurements of the surface pressure variation with time are compared in Fig. 12 to the theoretical variation as obtained from the momentum conservation expression which relates the pressure to the vehicle velocity and ambient density as follows:

$$p_w = K_3[K_4\rho V^{2.0}] \tag{6}$$

The bracketed quantity is the value that exists at the stagnation point and the factor K_3 accounts for the position of the orifice relative to the stagnation point. Once again the sinusoidal variation in the measurements has the same frequency as the vehicle spin rate with the amplitude essentially damped out near

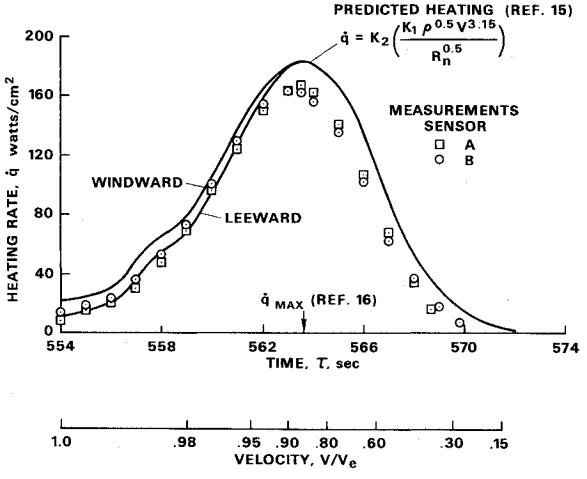

Fig. 11 Comparison of deduced PAET convective heating rates with laminar, equilibrium flow theory.

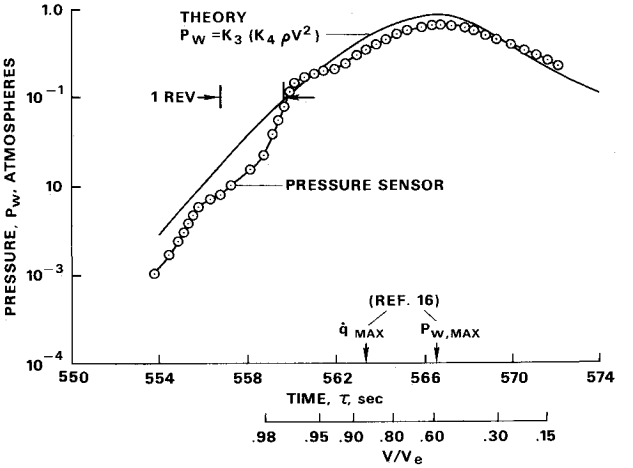

Fig. 12 Comparison of measured and predicted variation of surface pressure with time.

the time of peak heating. This latter observation confirms that the vehicle has achieved a constant-angle-of-attack attitude. The agreement of the predicted variation, which is based on an equation having a different power dependence on both velocity and density than that contained in the heating rate expression, with the measured variation provides still further evidence of the accuracy of the vehicle's trajectory variables and associated aeroheating environment. Furthermore, we may once again make use of the analysis of Allen and Eggers[16] to determine the velocity and altitude at which the pressure should attain its maximum value. The respective equations are

$$V/V_e = e^{-1/2} = 0.607 \tag{7}$$

$$h = h_s \ln (h_s \rho_{sl}/\beta \sin\theta_e) \tag{8}$$

The value of velocity corresponding to peak pressure as obtained from Eq. (1) is shown on the abscissa of Fig. 12. As was the case for the time peak heating, the agreement between the measured (566.8) and predicted (566.5) times are excellent. Using a scale height of 6.7 km in Eq. (8) the maximum pressure is calculated to occur at an altitude of 37.8 km. From Fig. 2, the altitude corresponding to a time of 566.8 sec is 36.4 km, which is within 3.6% of the predicted value.

Having precisely defined the ablator's boundary conditions of surface pressure and convective heating rate, which are both required to perform meaningful thermal response calculations, we conclude by comparing such predictions with the actual measurements made by the thermal sensors in the heat shields during the atmospheric entry of the PAET vehicle.

Heat-Shield Thermal Response

Forebody

Figure 13 shows predicted values and the measurements of temperature made on thermocouple plug C taken at 0.330 cm and 0.635 cm from the surface, and the single temperature measurement at position D, 0.24 cm from the surface. The calculations were performed by means of a finite difference computer program[2] which incorporates all the important surface energy accommodation mechanisms (reradiation, vaporization, combustion, and convective heat blockage), accounts for in-depth pyrolysis of the ablator, and assumes temperature dependence of all thermophysical properties of the material. The input heating conditions at the front surface used in the analysis were the theoretical values discussed in the previous section. The surface energy balance calculations revealed that 58% of the incident heat load was blocked by convection and the hot wall effect; of the remaining 42% incident on the surface, 29% was reradiated away, leaving only 13% of the total heat actually conducted into the interior of the material. The material degradation predicted for this heating showed that only 0.0036 cm of surface removal occurred throughout the entire heating pulse. This low level of recession, which was confirmed by laboratory tests (Appendix) at comparable levels of pressure and heating rate, means that the internal processes such as pyrolysis, as opposed to surface recession, governed the thermocouple response. The analysis indicated that the degradation front passed the position of the closest thermocouple at a time of 567 sec, and at the end of heating pulse the front had penetrated to a depth of 0.285 cm leaving 0.475 cm or approximately $\frac{6}{10}$ of the original thickness of undegraded, virgin material.

There are two possible reasons for the observed difference between the measured and predicted response of the thermocouple nearest the front surface. First, it is difficult to accurately measure the temperature in a region of the ablator where there is internal degradation in the form of vaporization accompanied by a related reduction in the local density and the formation of voids. Second, the kinetic model used in the analysis was developed for the entry of lifting bodies, which experience low levels of heating for prolonged periods of time (1000 sec). Although the analysis was supported by the performance of this ablator in such flights,[9] the applicability of a similar kinetic model to the transient heating history of PAET remains open to question and should be pursued in the laboratory.

To obtain the cooling characteristics of the forebody heat shield and to assure compatibility of the storage and engineering frame measurements, the output of the thermocouple in plug C at a depth of 0.330 cm was also transmitted in the engineering frame. The predicted values and measured responses of this thermocouple and the sensor monitoring the aluminium substructure to splashdown are presented in Fig. 14. Note the good agreement of the predicted and measured postheating-period decay of the forebody heat shield, which is goverened by the external cooling afforded by the ambient environment. This agreement supports the validity of the cooling model and indicates that the thermophysical properties of the virgin material, particularly conductivity and specific heat, are well characterized. The aluminium substructure temperature is rising, while that of the ablator, which is closer to the surface, is decreasing. The measured substructure temperature is slightly below the predicted value, which might be explained on the basis of the additional thermal mass provided by the aluminium lugs and micarta base plate. Near impact, the aluminium substructure temperature agrees with the heat-shield temperature, indicating that, as expected, thermal equilibrium has been achieved.

Afterbody

The performance of thermal protection materials in the regions of low-heating rates, characteristically the shoulders and afterbodies of re-entry vehicles, is not as efficient as in other regions of a spacecraft; such regions usually constitute a large fraction of

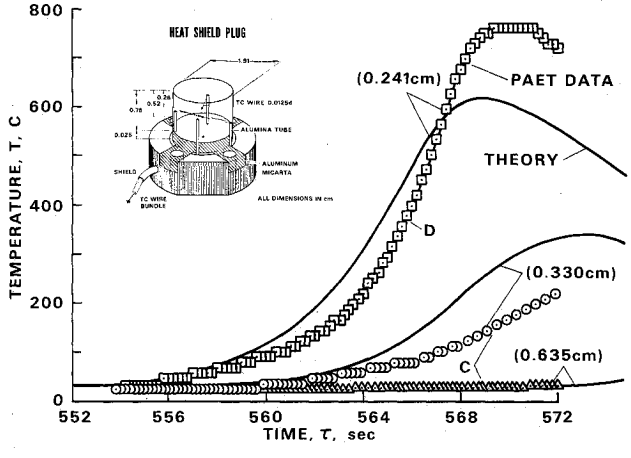

Fig. 13 Measured and predicted thermal response of PAET forebody heat-shield storage-frame data.

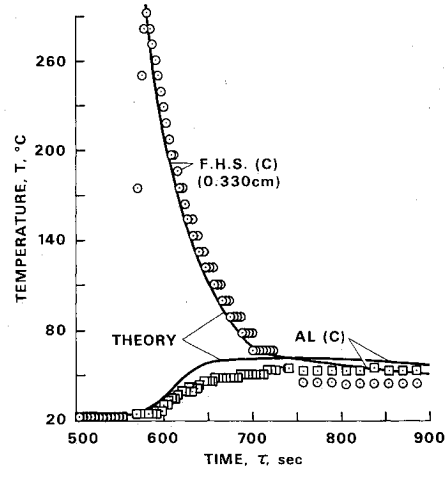

Fig. 14 Measured and predicted thermal response of PAET forebody heat-shield engineering-frame data.

the vehicle surface and, hence, weight of the thermal protection system. For this reason the response of ablators in the regions noted is of particular interest. In comparing the thermal response of the forebody and afterbody ablators, we first review the surface energy balance terms and associated thermal degradation predicted for the afterbody heat shield. Only 43% of the total incident heat load, which was 8% of that for the forebody, was blocked by the hot-wall effect and convection. Of the remaining 57% incident on the surface, 30% was reradiated away, leaving 27% to be conducted into the interior of the material. Because of the low heating level, the material is relatively inefficient; for example, no surface recession occurs and the calculated depth of pyrolysis was only 0.094 cm, leaving 0.594 cm, or approximately 85% of the original material in the virgin state.

The measured thermocouple response is compared with the predictions for the PAET vehicle in Fig. 15; the differences that occurred during the heating portions of the trajectory might be explained by the presence of a larger thermal mass in the region of the thermocouple, which would account for the lower measured temperature and the later peak. However, a detailed multilayer thermostructural analysis was formulated to account for 1) the additional face sheet and bond required for the thermocouple installation, 2) radiation between the face sheets of the honeycomb and the ground plane, and 3) the three-dimensional conduction paths. The calculations performed with the program[7] discounted the perturbation of lodal boundary conditions to the degree necessary to bring the predictions and measurements into good agreement. The validity of the analysis and the associated thermophysical properties of the ablator were verified by comparing the predictions with arcjet test results[17] obtained at heating rates of 8.6 and 18 w/cm^2 on a 27.9-cm-diam model. Agreement between the theory and data obtained at the ablator-honeycomb interface was found to be within 5% at both heating rates. The temperature rise for the higher rate at an exposure time of 10 sec was 90°C.

The other and most likely source of the observed difference is the magnitude of the convective heat-transfer rate $\dot{q}$ used in the calculations. The measured values ranged from 18% to 5% of the zero angle of attack, $\dot{q}_{s,\alpha=0}$, stagnation value on the windward ray and from 8% to 5% on the leeward ray, as the angle of attack was reduced from 25° to 0°. The variation of angle of attack with time was taken into account by treating $\dot{q}/\dot{q}_{s,\alpha=0}$ as a function of time. The average value for the results shown in Fig. 14 was approximately 8%. A set of calculations was performed to parametrically investigate the influence of the magnitude of $\dot{q}/\dot{q}_{s,\alpha=0}$ on the response of the afterbody ablator, assuming the ratio to be constant throughout the flight. The results indicate that the value in best agreement with the data observed in flight is 0.01 (Ref. 17). Although the forebody heating distributions determined in the tests of the scale model of the PAET were relatively insensitive to Reynolds number, the level of heating on the afterbody was found to decrease as the Reynolds number increased, but the scatter in the results and the fact that the model was sting mounted precluded any definitive conclusion. This finding is strengthened by the observations of Cassanto, who showed that the pressure (which affects heating) on the PAET afterbody, as determined from free-flight tests, was very sensitive to Reynolds number.[18] On the basis of these two sets of experiments, coupled with the flight data, it may be concluded that the incident cold-wall heat-transfer rate to the afterbody of the full-scale vehicle is likely to be considerably lower than the preflight estimates, which were based on wind-tunnel tests conducted at low Reynolds numbers. Furthermore, it must be remembered that the ground-based measurements were performed with a nonablating forebody and therefore should be conservative with respect to the flight situation in which ablation vapors from the forebody heat shield afforded downstream cooling in the afterbody region. The importance of forebody ablation on afterbody heating has been previously determined in the arc-jet tests of Lee and Sundell.[19] Although the vehicle was not recovered, reports on the visual sightings by personnel stationed on aircraft in the impact area (near Bermuda in the Atlantic Ocean) indicated that the vehicle, which was hydraulically stable in the afterbody-up attitude, was clearly distinguishable by the brilliance of the white afterbody. This observation is a qualitative indication that the charring and associated level of afterbody heating was low.

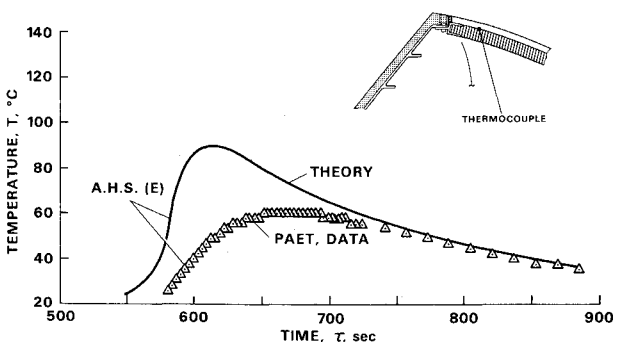

Fig. 15 Measured and predicted thermal response of PAET afterbody heat shield.

As was the case for the forebody ablation material, the agreement between the afterbody flight data and the predictions become extremely good with increasing time as the environment is controlled by the ambient temperature. This verification of the convective cooling model is of particular importance to missions such as the proposed Pioneer/Venus probe study now under way. For the probes entering the extremely dense and hot atmosphere of Venus, the thermal control problem is governed by the 1.5-hr descent time that follows the extremely brief (~6 sec) entry heating pulse.

Conclusions

A complete engineering experiment involving measurements of the aerodynamic heating and surface pressure, as well as in-depth temperature response of the heat shield materials, was carried out as part of the NASA Ames PAET flight project to evaluate the thermal environment and associated performance of two elastomeric heat-shield materials. From the findings of this experiment, the following conclusions have been reached.

1) The variation with time of both convective heat-transfer rate and surface pressure on the forebody were found to be within 5% of the respective variations predicted from ambient density and vehicle velocity as deduced from on-board instruments. In addition to accurately providing the environment of the forebody heat shield material, the heat-transfer data provided an extremely good check on the scale height of the atmosphere and, accordingly, the heat-transfer sensor can be considered a valuable backup instrument for atmospheric diagnostics.

2) Uncertainties in degradation kinetics are considered to be the source of the disagreement between the forebody heat-shield response and related predictions. On the other hand, the significant difference between the predicted and measured temperature of the afterbody heat-shield material is attributed to a milder environment than anticipated. Reasons for the environmental deviation from predicted values include lower inflight, cold-wall convective heat-transfer rates than the low Reynolds number test data used in the analysis; and downstream influence of forebody ablation vapors which reduced local heating to the afterbody in the region of the measurement.

3) The postheating cooling of both heat shield materials during the low-speed terminal phase of the descent, which is controlled by the ambient atmospheric temperature, was found to be predicted extremely well.

Appendix: Special Preflight Qualification Tests of Heat Shields

In addition to the laboratory tests carried out to define the convective heating distribution for the PAET configuration, two special experiments were undertaken to 1) provide preflight

verification of the ambient temperature sensor deployment through the forebody heat shield and, 2) define the RF characteristics of the afterbody heat-shield material. This appendix briefly describes the purpose, approach, and findings of these two experiments.

Evaluation of Ambient Temperature Sensor Deployment Procedure

The ambient temperature sensor[5,20] was designed to perform recovery temperature measurements of the atmosphere at low probe speeds. Since the sensor elements were uncooled the device was not capable of coping with the aerodynamic heating, and it was therefore necessary to deploy the instrument through the heat shield after heating had been encountered. The suggested approach shown schematically in Fig. 16 consisted of an initially compressed spring, which was released by a squib-fired cutter that severed a retaining screw. The motion of the spring, in turn, pushed out a protective plug of teflon located within a teflon insert in the heat shield, and inserted the instrument sensors into the flowing environment that enveloped the probe. A series of tests was performed to determine the force required to deploy the plug out of the assembly in its initially machined state; however, the critical question of whether the plug could be successfully deployed by the action of the spring following the heating pulse could only be answered by conducting the experiment.

A full-scale mockup of the actual flight hardware was mounted within a circular model holder, which was inserted into the 17.7 cm arc-heated wind-tunnel stream furnished by the NASA Ames Heat Transfer Tunnel. The stream enthalpy and flow rate were selected to provide a heating of 63.0 w/cm^2 and surface pressure of 0.11 atm, respectively. These values duplicated those predicted at the location of the two plugs situated symmetrically on the midpoint of the conical section on a plane 180° from the plane of the heat-shield plugs (see Fig. 6). Following a 20-sec exposure to these conditions, the arc was extinguished, and with the cold flow left on to simulate the flight conditions, the squib actuating the device was fired 7 sec later. High-speed motion pictures revealed that the plug was deployed at a velocity of approximately 4.7 m/sec. In addition to qualifying the deployment system the test also provided valuable information on the forebody ablator response. The over-all recession rate of the ablator was found to be only 0.003 cm even in the regions of highly localized heating: the teflon-ablator interface caused by the ablation of the teflon and the sharp model corner region which simulated the forebody-afterbody junction on the full-scale vehicle. These findings were of particular value in providing assurance that the discontinuity at the beryllium forebody ablator would not result in an adverse differential ablation.

Radio Frequency Transmission Tests of Afterbody Ablator

As noted earlier, the tracking antennas and VHF antennas for transmitting the flight data were located in the afterbody region. Because of this location of the antennas and the approximately 90° view angle from the receivers to the spacecraft relative to the vehicle axis of symmetry for both the Vanguard and Bermuda stations, the thermally degraded afterbody ablator had to be capable of transmitting the signals. Earlier tests to study such properties had been conducted on the PAET afterbody material and conventional polymeric ablators in an arc-heated wind-tunnel facility at the NASA Langley Research Center.[21] In contrast to the carbon-rich chars formed during the thermal degradation of conventional polymers, the silicaceous debris layer formed on the silicone-based materials during heating was found to transmit the incident signal with very little reduction in signal strength. However, some significant differences existed between the conditions of the earlier tests and the PAET configuration and anticipated environment.

The most significant differences were in the transmission frequency, the thickness and substructure of the ablator, and the level and duration of the heating pulse. In addition, to improve the handling qualities of the relatively fragile afterbody ablator, it was proposed to use a silicone-based paint (Dow Corning DC90-090), but the transmission characteristics of the paint-ablator combination were not known. In view of these differences, it was decided to perform a series of tests at Martin, which had available the required signal generator, and transmitting and receiving antennas, to define the RF transparency of the material, as well as determine the influence of the protective paint. A thermostructural model panel (36.6 cm × 35.6 cm) of the afterbody was heated by a bank of radiant lamps. The intensity of the lamps was controlled as a function of time in an attempt to produce the anticipated in-flight variation of surface temperature with time. The ratio of the transmitted to the incident signal was monitored as a function of time at three values of frequency (4, 5.5, and 8 GHz) for both painted and unpainted samples. The results of these six tests (Fig. 17) indicate that in all cases the transmission loss was less than the design limit of 1.5 db and that the transmission efficiency improved as the signal frequency was diminished. The addition of the paint resulted in a noticeable, but acceptable, reduction in the RF transmission response of the material. In some cases, the signal was strengthened as a result of the lens or focusing effect arising from the changes in both dielectric constant and index of refraction.[2] Furthermore, we note that the most pronounced changes in signal observed during the heating decreased considerably as the surface cooled. These laboratory findings were confirmed by the quality of the PAET data transmission, which remained relatively constant throughout the flight, except during the blackout period. The successful

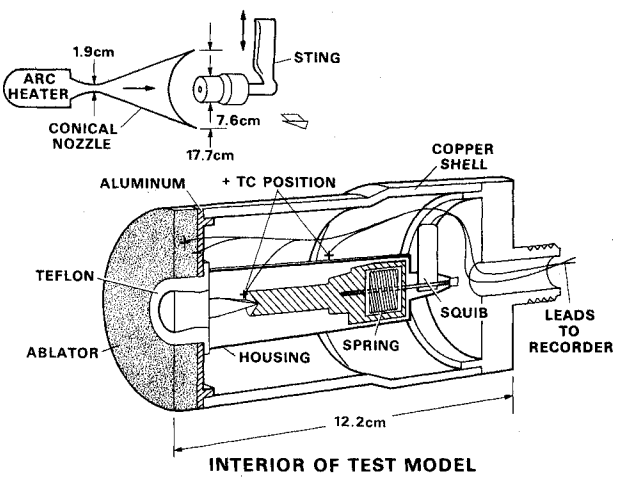

Fig. 16 Test setup for qualification of PAET ambient temperature sensor deployment mechanism.

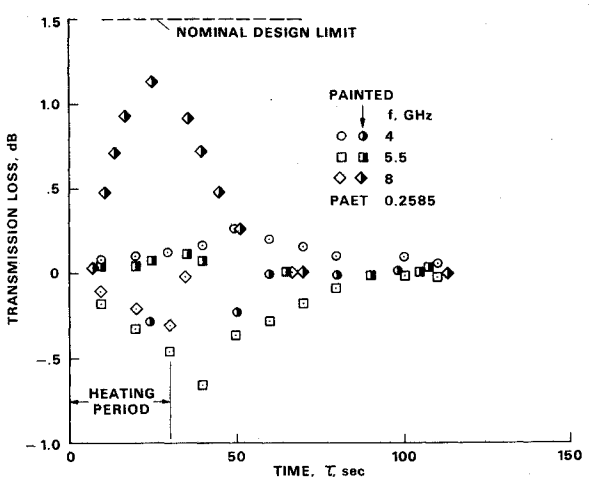

Fig. 17 Dependence of afterbody heat shield RF transmission on frequency and surface condition.

ground and flight qualification of the PAET afterbody ablator as an RF transparent material suggest additional applications such as antenna windows on the lee side of the Space Shuttle orbiter vehicle where the heating levels are comparable to those experienced on the PAET flight.

References

[1] Reese, D and Georgiev, S., "Design Problems and Experiments for Mars Atmospheric Probes," *Proceedings of AIAA/AES Stepping Stones to Mars Conference*, Baltimore, Md., March 1966, pp. 542–552.

[2] Carlson, D. L., "Heatshields for Planetary Atmospheric Experiments Tests," Final Rept., NAS 2-5538, Vol. I, Rept. MCR-70-170, May 1970, Martin Marietta Corp., Denver, Colo.

[3] Seiff, A., "Scientific Questions and Measurement Approaches for a Probe Entering the Atmosphere of Jupiter," Preprint AAS-71-148, presented at AAS 17th Annual Meeting, June 1971.

[4] Sommer, S. and Yee, L., "An Experiment to Determine the Structure of a Planetary Atmosphere," *Journal of Spacecraft and Rockets*, Vol. 6, No. 6, June 1969, pp. 704–710.

[5] Sommer, S. C., Boissevain, A. G., Yee, L., and Hedlund, R. C., "The Structure of an Atmosphere from On-Board Measurements of Pressure, Temperature, and Acceleration," TN D-3933, 1967, NASA.

[6] Linzer, F. D. and Kaplan, E., "Considerations in Design of Calorimeters for the Project FIRE Superorbital Re-Entry Test Vehicle," presented at SAE National Aeronautic and Space Engineering and Manufacturing Meeting, Los Angeles, Calif., Sept. 1963.

[7] Cornette, E. S., "Forebody Temperatures and Calorimeter Heating Rates Measured During Project FIRE II Reentry at 11.35 Kilometers per Second," TM X-1305, 1966, NASA.

[8] Rumsey, C. B., Carter, H. S., Hastings, E. C., Jr., Raper, J. L., and Zoby, E. V., "Initial Results from Flight Measurements of Turbulent Heat Transfer and Boundary Layer Transition at Local Mach Numbers Near 15 (Reentry F)," TM X-1856, 1966, NASA.

[9] "PRIME (Precision Recovery Including Manueverable Entry) Lifting Body Spacecraft," Air Force Rept. Vols. I and II, SAMSO-TR-68-11, May 1968, El Segundo, Calif.

[10] Dimeff, J., Lane, J. W., Deboo, G. J., and Hedlund, R. C., "A Vibrating Diaphragm Pressure Measuring System," *ISA Proceedings, 15 National Aerospace Instrumentation Symposium*, Las Vegas, Nev., May 1969, pp. 383–389.

[11] Lane, J. W. and Evans, R. D., "A High Altitude Altimeter Utilizing a Vibrating Diaphragm Transducer," ISA Paper 2.3.1, presented at the 16th National Instrument Society of American Aeronautics Institute Symposium, Seattle, Wash., May 1970.

[12] Stewart, D. A., "Convective-Heat-Transfer Rates on a Blunted 110° Cone with Hemispherical Afterbody at Hypersonic Speeds," TN D-6433, 1971, NASA.

[13] Kemp, N. H., Rose, P. H., and Detra, R. W., "Laminar Heat Transfer Around Blunt Bodies in Dissociated Air," Research Rept. 15, 1958, AVCO Research Lab., Everett, Mass.

[14] Howard, F. G., "Single-Thermocouple Method for Determining the Heat Flux to a Thermally Thick Wall," TN D-4737, 1968, NASA.

[15] Detra, R. W., Kemp, N. H., and Riddell, F., "Addendum to Heat Transfer to Satellite Vehicles Re-Entering the Atmosphere," *Jet Propulsion*, Vol. 21, No. 12, Dec. 1957, pp. 1256–1257.

[16] Allen, H. J. and Eggers, A. J., "A Study of the Motion and Aerodynamic Heating of Ballistic Missiles Entering the Earth's Atmosphere at High Supersonic Speeds," TR-1381, 1958, NACA.

[17] Carlson, D. L., "PAET Afterbody Thermal Performance and Component Structural Properties," (NAS 2-6274) CR-114293, 1971, NASA.

[18] Cassanto, J. W., "An Experiment to Determine the Atmospheric Pressure Profile of a Plant Using Base Pressure Measurements," AIAA Paper 72-202, San Diego, Calif., 1972.

[19] Lee, G. and Sundell, R., "Apollo Afterbody Heat Transfer and Pressure with and without Ablation at $M = 5.8$ to 8.3," TN D-3620, 1966, NASA.

[20] Millard, J. P., Green, M. J., and Sommer, S. C., "Analytical Design of Sensors for Measuring Atmospheric Temperature During Planetary Entry," TN D-6947, 1972, NASA.

[21] Gilreath, M. C., Chapman, A. J., and Hatcher, D. M., "Radio-frequency Transmission Characteristics of Candidate Ablation Materials for Planetary-Entry Vehicle Heat Shields," TN D-4920, 1968, NASA.